Sensors and Actuators B 221 (2015) 305–311

Contents lists available at ScienceDirect

Sensors and Actuators B: Chemical

journal homepage: www.elsevier.com/locate/snb

Mass and force sensing of an adsorbate on a string resonator

Yin Zhang*, Ya-Pu Zhao

State Key Laboratory of Nonlinear Mechanics (LNM), Institute of Mechanics, Chinese Academy of Sciences, Beijing 100190, China

ARTICLE INFO

Article history:
Received 1 April 2015
Received in revised form 4 June 2015
Accepted 5 June 2015
Available online 2 July 2015

Keywords:
String
Resonator
Sensing
Inverse problem
Resonant frequency

ABSTRACT

The shift of resonant frequency is the sensing mechanism for a mechanical resonator. The adsorbate mass, position and induced force are the three dominant things responsible for the resonant frequency shifts of a string resonator. In the application of a resonator sensor, the (shifts of) resonant frequencies are the measured quantities and therefore, an inverse problem arises naturally: How to determine the adsorbate mass, position and induced force by the resonant frequencies? An inverse problem solving method on the string resonator with one adsorbate is presented and its accuracy is demonstrated. How the method can be used in a real string sensor application scenario is also discussed.

1. Introduction

Because of the high mass sensitivity and frequency stability, micro/nanomechanical resonator [1] is suitable for detecting tiny mass. One important technical parameter for evaluating the micro/nanomechanical resonator performance, which is also a major driving force for its development, is the minimum detectable mass [5]. The ultimate goal is to resolve a single quantum of a measured quantity [6]. With the enormous efforts on both the device fabrication and readout technologies, in 2012, a carbon nanotube based nanomechanical resonator achieved the mass resolution of less than one yocotogram ($1\,yg = 10^{-24}\,g$) [7]. The nanomechanical resonator with the one yocotogram resolution is capable of chemical and even isotopic identification [8] because the mass of a proton is around 1.65 yg. The ultimate mass resolution limit of a nanomechanical resonator is imposed by the thermomechanical fluctuations, which is proven to be well below a yocotogram [1]. Many advantages of the mass sensing based on nanomechanical resonator over mass spectrometry have been demonstrated [9–11]. Mass spectrometry has been an essential tool in proteomics for the rapid and quantitative analysis of cellular systems [12] and protein identification [13,14]. Because mass spectrometry measures the mass-to-charge and charges, the ionization or acceleration stage in a chamber may damage or even destroy the fragile analytes such as biological macromolecules or proteins [15,16]. In comparison, the working mechanism of a micro/nanomechanical resonator is the shifts of resonant frequencies (eigenfrequencies) due to an accretion, which allows it to work with neutral species [9,10]. Micro/nanomechanical resonator has been providing a rapid, high-throughput and label-free detection of biological and chemical molecules [17].

When an analyte is adsorbed, a mechanical resonator generally experiences three changes in mass, stiffness and damping [18,19], which all lead to the shifts of resonant frequencies. Damping indicates the energy dissipation of a resonator and it is a known parameter because it can be experimentally determined from the frequency response curve [19,20]. The reason for the mass change is obvious. However, the adsorbate position also plays an important role together with its mass in the shifts of resonant frequencies [9–11,17]. In the application of nanomechanical resonator, detecting the adsorbate position is extremely difficult or even impossible when an adsorbate is as small as a protein [9,10], a molecule [7,17] and an atom [8,11]. The stiffness change due to adsorption can result from many sources, for example, surface stress [19,21], the adsorbate stiffness [22–24], the stress variation [3,25–27], the alloy formation [28,29], swelling [30] and polymer chains interpenetrated by small adsorbate molecules [31], etc. In one word, a lot of things can occur with adsorption, which is the very reason making the interpretation on adsorption "notoriously difficult" [7]. In logics terms, the changes of mass, stiffness and damping are the causes and the shifts of resonant frequencies are the effects. In the forward problem of a mechanical resonator, once those parameters concerning the causes are given, the effects of the resonant frequency shifts are uniquely determined [19,24]. However, in the

* Corresponding author. Tel.: +86 01082543970.
E-mail address: zhangyin@lnm.imech.ac.cn (Y. Zhang).

http://dx.doi.org/10.1016/j.snb.2015.06.047
0925-4005/

real application of mechanical resonator, the resonant frequencies and their shifts are the measured quantities. Therefore, solving the inverse problem, i.e., how to link the effects to the causes, is "the most important problem" [15] in the mechanical resonator applications [7,9–11,21]. When the number of the parameters concerning the causes is two or larger, there are infinite combinations of these parameters which can result in the same shift of one resonant frequency [19,24]. To extract each one of the parameters from the resonant frequencies, which are dependent on those convolved parameters, is key to the nanomechanical resonator application [9,10]. When the number of (unknown) parameters is one, the (shift of) resonant frequency has the one-to-one relation with the parameter. By assuming an adsorbate at the center or the free end of a carbon nanotube [32,33] and a carbon nanocone [34], the only unknown parameter of the adsorbate mass is uniquely determined as a monotonic function of the resonant frequency. Kehrbusch et al. [35] fabricated the vertically aligned silicon resonator and as a result, adsorbates can only land on the top of the column. When both position and mass of an adsorbate are unknown, two or more resonant frequencies are needed to identify the two parameters [9,10,26,36,37]. Even for this two-parameter case, solving the inverse problem is not an easy task: complex statistics [9,10], algorithm [36] and graphic solution [26,37] methods are used. In this study, one more parameter is added: the adsorbate-induced stress. There are various mechanisms causing the stress variation inside a nanomechanical resonator. For example, the resonator built-in tensile stress can be relieved by adsorbate absorbing light (photothermal effect) [3], distorting lattice [25,26] and hydroxylation [27], etc. Sometimes the force or stress variation even dominates the shifts of resonant frequencies, which has been used as the sensing mechanism for hydrogen [25] and various ions [27]. In this study, a generalized method of solving the inverse problem is presented for a string resonator. In the previous studies [4,7–11,26,36], the mechanical resonators are for mass sensing only. By incorporating the adsorbate-induced force in the model, the force sensing function is added. Also, in previous studies, damping is explicitly or implicitly ignored for simplicity reason. Higher accuracy can be achieved by including damping in the model. With the presence of damping, finding the resonant frequencies (eigenfrequencies) is not an easy task because those eigenfrequencies are complex numbers and special mathematical manipulation is needed to solve the eigenvalue problem. A much simpler approximate analytical solution to the eigenfrequencies is thus derived and its accuracy is also demonstrated. The inverse solving method presented in this study should be some help for the string resonator sensor to have a better characterization on the effects of an adsorbate.

For a hinged-hinged beam under an axial load, its nth (angular) eigenfrequency, f_n, is given as follows [38]

$$f_n = \frac{(n\pi)^2}{L^2}\sqrt{\frac{EI}{\rho A}}\sqrt{1+\frac{TL^2}{(n\pi)^2 EI}} \tag{1}$$

where L, A and I are the beam length, cross-section area and moment of inertia, respectively. E is the beam effective Young's modulus and T is the axial load. When the axial load is tensile ($T>0$) and $TL^2/(n\pi)^2EI \gg 1$, the above equation can be written as the following:

$$f_n = \frac{n\pi}{L}\sqrt{\frac{\sigma}{\rho}} \tag{2}$$

where $\sigma = T/A$ is the tensile stress. Eq. (2) is the nth eigenfrequency of a string. Wei et al. [39] observed that when $TL^2/\mathrm{EI} > 2000$, a carbon nanotube vibrates as a string rather than a beam; Unterreithmeier et al. [40] also found that when $\sigma > 100$ MPa, the stretching energy of a silicon nitride nanowire is dominant and the bending energy becomes negligible, which means the string behavior dominates. Many one-dimensional mechanical resonators are modeled as a string because of the presence of large tension [3,4,8,25]. The above two equations essentially say one thing: when tension is large, a beam behaves like a string. However, from the perspective of a mechanical resonator, there is more to tell. As seen in the Eq. (1), the presence of tension increases resonant frequencies, which is helpful to the resonator sensitivity [15,26]. A micro/nanomechanical resonator can take much larger tensile stress without failure than a macroscopic one. For example, the silicon nitride nanowire in the experiments is under the tensile stress of 830 MPa [40] and 1.4 GPa [41], respectively. Tension is also an important mechanism to tune the resonant frequency, which is crucial for the resonator application [42]. Small damping, or say, large quality factor, is a much sought-after property in a mechanical resonator [40,41,43,44], which is a key factor of determining the sensitivity [26]. Recently, the quality factor with the record high value of five million was achieved in a carbon nanotube mechanical resonator [43]. Tensile stress can significantly enhance the quality factor of a mechanical resonator [26,40,41,43,44]. One possible mechanism is that increasing tension may enlarge the acoustic mismatch between the string resonator and support; as a result, the energy dissipation due to clamping loss is mitigated [41]. High tensile stress also leads to high mechanical stability [40]. Slack may occur in a suspended one-dimensional mechanical resonator [45] and it can induce nonplanar motion, i.e., whirling [46] or the so-called jump-rope mode [47], which makes the analysis extremely difficult. Exerting tension is an effective way of eliminating slack. Compared with a string resonator, there are two more quantities for a beam resonator: E and I, which sometimes can be extremely difficult to be characterized for a micro/nanomechanical resonator. Because of its small size, the mechanical properties (including E) of a micro/nanoresonator are prone to the microstructure defect, grain morphology, impurities [2,44], surface [48] and nonlocality [49] effects, etc. Furthermore, a micro/nanomechanical resonator is often coated with some material, which makes the resonator a composite structure [42]. Because of the smaller size, the coating layer is more sensitive to defects and it is more difficult to characterize its thickness (in order to get I). The residual stress inside the coating layer [42], which also plays an important role in the stiffness of the composite structure, makes the characterization further difficult. Because of the device-to-device variations, it is not uncommon that for some nanomechanical sensors, the reproducible results cannot be obtained [16]. By exerting high tension, not only a resonator can achieve a better performance but also we don't have to characterize some parameters which are among the most difficult ones to be measured.

2. Model development

Fig. 1(a) is the schematic of an adsorbate on a carbon nanotube (CNT)-based resonator with the length of L. When a resonator is under a large tension, the following string model applies [4]

$$[m + M_o\delta(x-x_o)]\frac{\partial^2 w}{\partial t^2} + c\frac{\partial w}{\partial t} - (T+\Delta T)\frac{\partial^2 w}{\partial x^2} = 0. \tag{3}$$

where $m = \rho A$ is the resonator mass per unit length; w is the string transverse displacement; c is the damping; M_o and x_o are the mass and position of the adsorbate, which is modeled as a concentrated mass by the Dirac delta function of δ [50,51] because its size is (very) small compared with that of the resonator. T is the tension and ΔT is the corresponding variation due to the adsorbate.

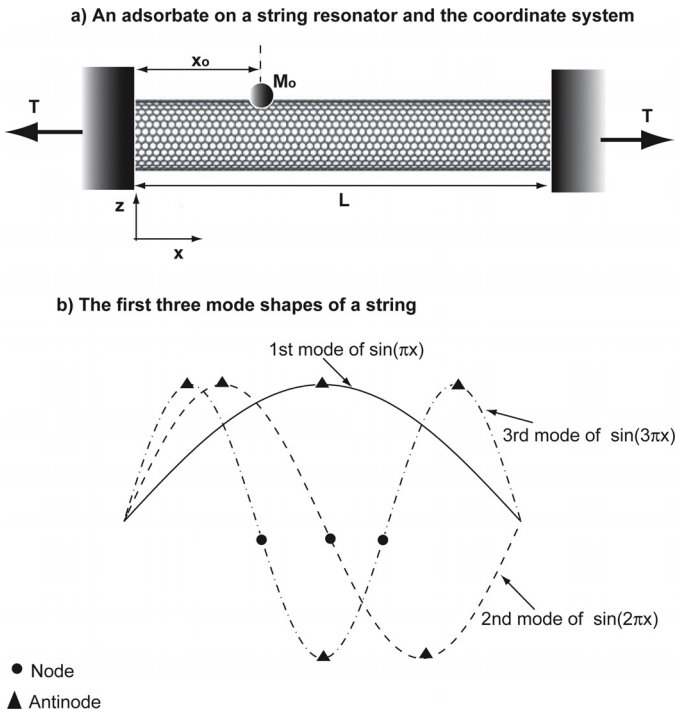

Fig. 1. (a) Schematic diagram of an adsorbate on a carbon nanotube-based resonator modeled as a string. (b) The first three mode shapes of a string, which are $\sin(\pi\xi)$, $\sin(2\pi\xi)$ and $\sin(3\pi\xi)$, respectively. The nodes which correspond to zero modal displacement are marked with solid circles; and the antinodes which correspond to the maximal modal displacements are marked with solid triangles.

By introducing $\xi = x/L$, $\tau = \sqrt{T/(mL^2)}t$ and $W = w/L$ [20], Eq. (3) is nondimensionalized as follows:

$$[1+\alpha\delta(\xi-\xi_o)]\frac{\partial^2 W}{\partial\tau^2} + C\frac{\partial W}{\partial\tau} - (1+\beta)\frac{\partial^2 W}{\partial\xi^2} = 0. \tag{4}$$

where the dimensionless parameters α, β, ξ_o and C are defined as the following

$$\alpha = \frac{M_o}{mL}, \quad \beta = \frac{\Delta T}{T}, \quad \xi_o = \frac{x_o}{L}, \quad C = c\frac{L^2}{T}\sqrt{\frac{T}{mL^2}}. \tag{5}$$

Physically, α is the mass ratio of the adsorbate to the resonator and $\alpha \geq 0$; β is the variation ratio of tension and β can be either positive or negative or zero. Here positive β means that the tension is enhanced and negative β means that the tension is reduced. $\xi_o = x_o/L$ is the dimensionless adsorbate location. C is the dimensionless damping; and from the above definition, it is not hard for us to derive the following relation of $C = \pi/Q$, where Q is the quality factor (of the string first mode).

Here the Galerkin method is applied for the eigenfrequency computation, which assumes the following form for $W(\xi, \tau)$ [50]

$$W(\xi,\tau) = \sum_{j=1}^{N} a_j(\tau)\phi_j(\xi) = \sum_{j=1}^{N} a_j(\tau)[\sqrt{2}\sin(j\pi\xi)], \tag{6}$$

where N is the mode number and $a_j(\tau)$ is the unknown jth modal amplitude. $\phi_j(\xi)$ is the jth mode of a string, which corresponds to $\phi_j(\xi) = \sqrt{2}\sin(j\pi\xi)$. The first three mode shapes are presented in Fig. 1(b). The purpose of introducing the factor of $\sqrt{2}$ is to have the following orthonormal relation

$$\int_0^1 \phi_i\phi_j d\xi = \delta_{ij} = \begin{cases} 0, & i \neq j \\ 1, & i = j. \end{cases} \tag{7}$$

where δ_{ij} the Kronecker delta function. Now substitute Eq. (6) into Eq. (4), time $\phi_i(\xi)$ and integrate from 0 to 1, the following governing equations are derived

$$\mathrm{M}\ddot{\mathrm{q}} + \mathrm{D}\dot{\mathrm{q}} + \mathrm{K}\mathrm{q} = \mathbf{0}. \tag{8}$$

Here $\dot{(\,)} = \frac{\partial}{\partial\tau}$ and $\mathbf{q}$ is the vector defined as $\mathbf{q} = (a_1, a_2, \ldots, a_N)^T$. $\mathbf{M}$, $\mathbf{D}$ and $\mathbf{K}$ are the $N \times N$ matrices of mass, damping and stiffness, respectively, which are derived as the following by using both the orthonormality property of $\phi_j(\xi)$ and the integration property of the Dirac function [50,51]

$$\mathbf{M}_{ij} = \delta_{ij} + 2\alpha\sin(i\pi\xi_o)\sin(j\pi\xi_o), \quad \mathbf{D}_{ij} = C\delta_{ij}, \quad \mathbf{K}_{ij} = (1+\beta)j^2\pi^2\delta_{ij}. \tag{9}$$

Because Eq. (8) is a damped nongyroscopic system, it needs to be rewritten as the following form to formulate an eigenvalue problem [52]

$$\mathrm{M}^*\dot{\mathrm{v}} + \mathrm{K}^*\mathrm{v} = \mathbf{0}. \tag{10}$$

where $\mathbf{v} = (\dot{\mathrm{q}}, \mathbf{q})$ is a $2N$ vector; $\mathbf{M}^*$ and $\mathbf{K}^*$ are the $2N \times 2N$ matrices defined as follows [52]

$$\mathrm{M}^* = \begin{pmatrix} \mathbf{M} & \mathbf{0} \\ \mathbf{0} & -\mathrm{K} \end{pmatrix}, \quad \mathrm{K}^* = \begin{pmatrix} \mathbf{D} & \mathbf{K} \\ \mathbf{K} & \mathbf{0} \end{pmatrix} \tag{11}$$

By letting $\mathbf{v}(\tau) = e^{i\omega\tau}\mathbf{V}$, Eq. (10) formulates a standard eigenvalue problem of $\mathbf{AV} = i\omega\mathbf{V}$ with $\mathbf{A} = -(\mathrm{M}^*)^{-1}\mathrm{K}^*$ [52]. Because of the presence of damping, the eigenvalue of ω is a complex variable of $\omega = R + iI$. The real part (R) is the eigenfrequency and the imaginary part (I) indicates the stability of the system [53]. When an adsorbate is not located at the ends or nodes (i.e., $\sin(j\pi\xi_o) = 0$), there are off-diagonal elements in the mass matrix as seen in Eq. (9). There is no analytical solution to Eq. (10) and numerically solving the eigenvalue problem of Eq. (10), by any standard, is not an easy task. Here an approximate solution is derived, which is shown to be accurate when α is small [50] and the complexity of solving Eq. (10) can thus be avoided.

By assuming $W = \sum_{j=1}^{N} b_j e^{i\omega\tau}(\tau)\phi_j(\xi)$ ($\omega = R + iI$) and repeating the same procedure of Galerkin method above, the following equation is derived

$$\mathbf{GB} = 0. \tag{12}$$

where $\mathbf{G}$ is a $N \times N$ complex matrix given as $\mathbf{G}_{ij} = \mathbf{G}^r_{ij} + i\mathbf{G}^i_{ij}$ and $\mathbf{B}$ is a vector defined as $\mathbf{B} = (b_1, b_2, \ldots b_N)^T$. The real part ($\mathbf{G}^r_{ij}$) and imaginary part ($\mathbf{G}^i_{ij}$) are given as the following

$$\mathbf{G}^r_{ij} = (1+\beta)j^2\pi^2\delta_{ij} - IC\delta_{ij} - (R^2 - I^2)[\delta_{ij} + 2\alpha\sin(i\pi\xi_o)\sin(j\pi\xi_o)],$$
$$\mathbf{G}^i_{ij} = RC\delta_{ij} - 2RI[\delta_{ij} + 2\alpha\sin(i\pi\xi_o)\sin(j\pi\xi_o)] \tag{13}$$

To have nontrivial solution of $\mathbf{B}$, the determinants of both real part $\mathbf{G}^r_{ij}$ and imaginary part $\mathbf{G}^i_{ij}$ must be zero. Therefore, $\det(\mathbf{G}^r_{ij}) = 0$ and $\det(\mathbf{G}^i_{ij}) = 0$ formulate the eigenvalue problem for R and I, which actually is equivalent to solving Eq. (10) and can only be done numerically. However, if the off-diagonal elements are ignored, $\det(\mathbf{G}^r_{ij}) = 0$ and $\det(\mathbf{G}^i_{ij}) = 0$ lead to the following two equations

$$\begin{cases} (1+\beta)j^2\pi^2 - IC - (R^2 - I^2)[1 + 2\alpha\sin^2(j\pi\xi_o)] = 0, \\ C - 2I[1 + 2\alpha\sin^2(j\pi\xi_o)] = 0. \end{cases} \tag{14}$$

R and I are thus analytically obtained as the following

$$R_j = \sqrt{\frac{(1+\beta)j^2\pi^2}{1 + 2\alpha\sin^2(j\pi\xi_o)} - \frac{C^2}{4[1 + 2\alpha\sin^2(j\pi\xi_o)]^2}}, \tag{15}$$

$$I_j = \frac{C}{2[1 + 2\alpha\sin^2(j\pi\xi_o)]^2}. \tag{16}$$

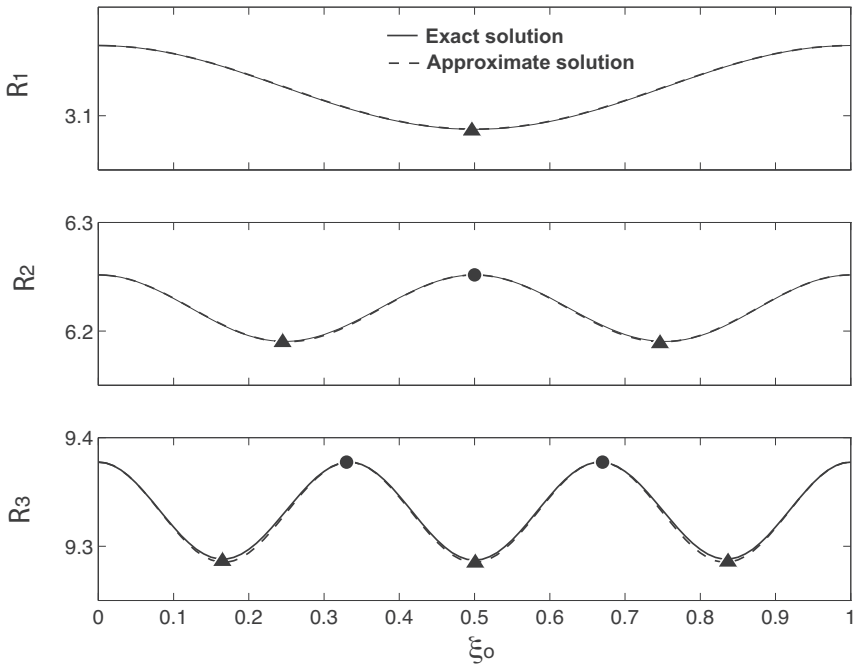

Fig. 2. The comparison of the first three resonant frequencies computed by Eq. (10) (solid line, exact solution) and by Eq. (15) (dashed line, approximate solution) as the adsorbate dimensionless location of ξ_o varies from 0 to 1. Here $\alpha = 10^{-2}$, $\beta = -10^{-2}$ and $C = 10^{-3}$ are fixed.

When $\alpha = \beta = C = 0$, $R_j = R_j^o = j\pi$ recovers the classical solution of the jth eigenfrequency of a string with no damping and adsorbate [20]; when $\beta = C = 0$, $R_j = R_j^o/\sqrt{1 + 2\alpha\sin^2(j\pi\xi_o)}$ is the dimensionless form of Schmid's Eq. (6), which was obtained by an energy method [4].

Fig. 2 presents the comparison of the first three eigenfrequencies computed by Eqs. (10) and (15) as the adsorbate moves from one end to the other. In Fig. 2, $\alpha = 10^{-2}$, $\beta = -10^{-2}$ and $C = 10^{-3}$ are set. The variations of the three eigenfrequencies correspond to their mode shapes as plotted in Fig. 1(b). In Figs. 1(b) and 2, the antinodes, where the modal displacements are maximum, are marked with the solid triangles; the nodes, where the modal displacements are zero, are marked with the solid circles. The effect of the adsorbate mass maximizes at the antinodes, which leads to the minimum eigenfrequencies. On the other hand, the effect of the adsorbate mass becomes zero at the nodes, the eigenfrequencies are the maximum and equal to those at the ends. The computation differences between Eqs. (10) and (15) maximize at the antinodes. The corresponding maximum computation differences of the first, second and third eigenfrequencies are 0.0024%, 0.0056% and 0.0321%, respectively. When the adsorbate mass (α) is small (which is often the case in the resonator applications), the off-diagonal elements of the mass matrix have little impact on the eigenfrequency computation and Eq. (15) is thus accurate. Compared with Eqs. (10) and (15) is an approximate analytical solution capable of providing the straightforward and fast computation on the eigenfrequencies, which is important for the real-time mass spectrometry application [4].

3. Results and discussion

We present two cases on how to use Eqs. (10) and (15) to solve the inverse problem. In the forward (direct) problem, for Eq. (10) or Eq. (15) to work, α, ξ_o, β and C must be supplied. The damping, C, can be found by the so-called half-power method from the experimentally measured frequency response curve [19,20]. However, in the real application of a resonator sensor, resonant frequencies are the measured quantities; α, ξ_o and β are the unknowns to be determined. In the first case, $\alpha = 10^{-2}$, $\xi_o = 0.4$, $\beta = -10^{-2}$ and $C = 10^{-3}$ are set. Once these parameters are given, the (exact) first three eigenfrequencies are uniquely determined by Eq. (10) as the following

$$R_1 = 3.09783, \quad R_2 = 6.23047, \quad R_3 = 9.34562. \tag{17}$$

Because of the presence of mass, damping and negative β, which relieves tension [25,27] and thus reduces the stiffness, all the three eigenfrequencies have the relation of $R_j < R_j^o$ ($R_j^o = j\pi$ is the jth eigenfrequency with $\alpha = \beta = C = 0$ [20]). Here we define $\Delta_j = (R_j - R_j^o)/R_j^o$ as a quantity to indicate the relative shift of each eigenfrequency and the corresponding equation of Eq. (17) is as follows:

$$\Delta_1 = -1.39\%, \quad \Delta_2 = -0.84\%, \quad \Delta_3 = -0.84\%. \tag{18}$$

In a real application, the above R_js are the (known) measured quantities. In order to present a graphic illustration on how the inverse problem is solved, for the time being, we assume that $\beta = -10^{-2}$ is a known quantity. Now there are only two unknowns: α and ξ_o.

Fig. 3(a) presents the variation of the first resonant frequency (R_1) as the function of α and ξ_o. Here α varies from 0 to 0.02; ξ_o varies from 0 to 0.5. As seen in Fig. 2, because of the symmetry of the structure, the adsorbate mass induces the same eigenfrequency variation at ξ_o and $1 - \xi_o$. Therefore, we only search the adsorbate location in $0 \le \xi \le 0.5$. The really useful quantities in a resonator sensor measurement are the adsorbate mass and induced force, not its location. In this case, it does not matter whether the adsorbate locates at ξ_o or $1 - \xi_o$ because it has no impact on the measurement of α and β. The level plane is the one with $R_1 = 3.09783$. The intersection of the two planes are marked with a solid line. Physically, this solid line means that there are infinite combinations of α and ξ_o resulting the same first resonant frequency of $R_1 = 3.09783$. Fig. 3(b) presents the variation of the second resonant frequency (R_2) as the function of α and ξ_o. The level plane is the one with $R_2 = 6.23047$. Again, the intersection of the two planes is the infinite combinations of α and ξ_o resulting the same second resonant frequency of $R_2 = 6.23047$, which is marked a dashed line. In contrast, once α, ξ_o, β and C are given, each eigenfrequency (R_j) is uniquely determined by

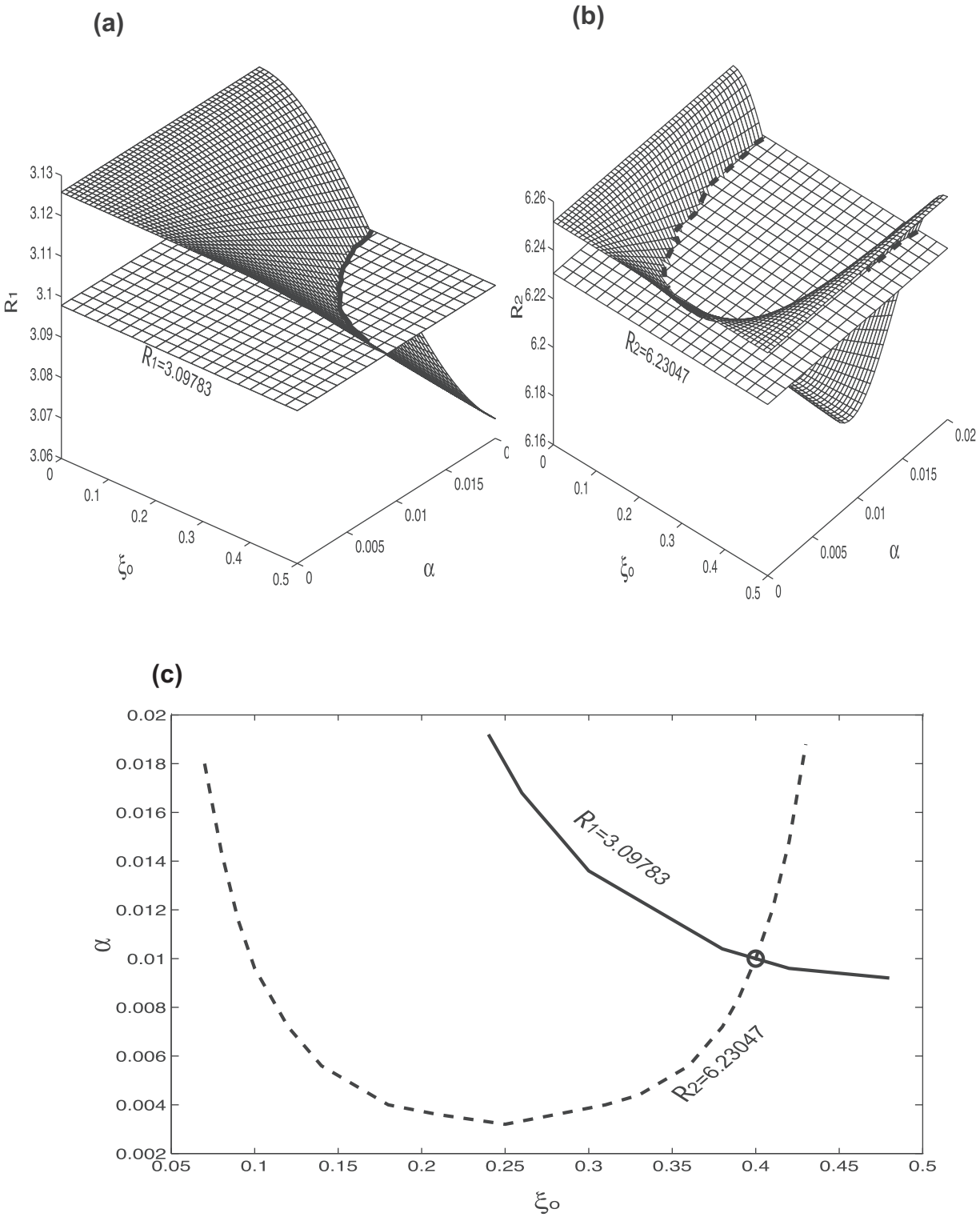

Fig. 3. (a) The variation of the first resonant frequency (R_1) as a function of α and ξ_o, which are the adsorbate dimensionless mass and location, respectively. The level plane is the one with the constant of $R_1 = 3.09783$. The intersection of the two planes is marked with a solid curve. Here $\beta = -10^{-2}$ is fixed. (b) The variation of the second resonant frequency (R_2) as a function of α and ξ_o. The level plane is the one with the constant of $R_2 = 6.23047$. The intersection of the two planes is marked with a dashed curve. (c) The projections of the two intersection curves obtained in (a) and (b) into the $\alpha - \xi_o$ plane. The intersection of the two curves is marked with a circle, which corresponds to (α, ξ_o)=(0.01, 0.4) exactly.

Eq. (10) as a forward problem. When these two curves obtained in Fig. 3(a) and (b) are projected into the $\xi_o - \alpha$ plane, they intersect and in Fig. 3(c) the intersection point is marked as a circle, which is exactly (α, ξ_o)=$(10^{-2}, 0.4)$. Physically, the reason for the two curves to intersect is the following mechanism: α and ξ_o have different impacts on different resonant frequencies; different resonant frequency responds differently to the given α and ξ_o. The similar physical mechanism also helps to solve a different type of inverse problem [54], in which surface stress and surface elasticity are the two unknowns.

Mathematically, as seen in the mass matrix of Eq. (9), α is a coefficient and ξ_o is embedded in the mode shape of sine function.

In fact, Eq. (10) has the function form of $\mathcal{F}(R_j, \alpha, \xi_o, \beta, C) = 0$. In the forward problem, α, ξ_o, β and C are supplied to compute the eigenfrequency of R_j. In the above inverse problem, R_j, β and C are known, the only two unknowns are α and ξ_o. The above graphic illustration on the inverse problem solving procedure presented in Fig. 3 can be succinctly summarized as solving the following two nonlinear equations

$$\begin{cases} \mathcal{F}(R_1, \alpha, \xi_o, \beta, C) = \mathcal{F}(3.09783, \alpha, \xi_o, -10^{-2}, 10^{-3}) = 0, \\ \mathcal{F}(R_2, \alpha, \xi_o, \beta, C) = \mathcal{F}(6.23047, \alpha, \xi_o, -10^{-2}, 10^{-3}) = 0. \end{cases} \tag{19}$$

Eq. (19) provides two (nonlinear) equations to solve the two unknowns of α and ξ_o. When the Newton–Raphson method [55] is applied, the exact solution of (α, ξ_o)=$(10^{-2}, 0.4)$ is obtained. In general, β is also unknown and there are three unknowns in total, which requires three equations to be solved. The third equation can be provided by measuring the third eigenfrequency of R_3, which is presented as follows

$$\begin{cases} \mathcal{F}(R_1, \alpha, \xi_o, \beta, C) = \mathcal{F}(3.09783, \alpha, \xi_o, \beta, 10^{-3}) = 0, \\ \mathcal{F}(R_2, \alpha, \xi_o, \beta, C) = \mathcal{F}(6.23047, \alpha, \xi_o, \beta, 10^{-3}) = 0, \\ \mathcal{F}(R_3, \alpha, \xi_o, \beta, C) = \mathcal{F}(9.34562, \alpha, \xi_o, \beta, 10^{-3}) = 0. \end{cases} \tag{20}$$

Now Eq. (20) provides three nonlinear equations to solve three unknowns of α, ξ_o and β. Once again, the Newton-Raphson method is applied and the exact solution of (α, ξ_o, β)=$(10^{-2}, 0.4, -10^{-2})$ is also obtained.

Similarly, Eq. (15) can be rewritten into the following function form of $\mathcal{G}(R_j, \alpha, \xi_o, \beta, C) = R_j - \sqrt{(1+\beta)j^2\pi^2/[1+2\alpha\sin^2(j\pi\xi_o)] - C^2/\{4[1+2\alpha\sin^2(j\pi\xi_o)]^2\}} = 0$. The following three equations can now be presented for solving the inverse problem

$$\begin{cases} \mathcal{G}(R_1, \alpha, \xi_o, \beta, C) = \mathcal{G}(3.09783, \alpha, \xi_o, \beta, 10^{-3}) = 0, \\ \mathcal{G}(R_2, \alpha, \xi_o, \beta, C) = \mathcal{G}(6.23047, \alpha, \xi_o, \beta, 10^{-3}) = 0, \\ \mathcal{G}(R_3, \alpha, \xi_o, \beta, C) = \mathcal{G}(9.34562, \alpha, \xi_o, \beta, 10^{-3}) = 0. \end{cases} \tag{21}$$

The Newton–Raphson method yields the solution of (α, ξ_o, β)= $(1.014\times10^{-2}, 0.4000062, -9.8265\times10^{-3})$. Compared with the exact solution of (α, ξ_o, β)=$(10^{-2}, 0.4, -10^{-2})$, the corresponding errors of α, ξ_o and β are 1.4%, 0.0154% and 1.7344%, respectively. The error mainly results from the approximation of Eq. (15) by eliminating the off-diagonal elements.

In the above examples, the exact "measured" resonant frequencies of Eq. (17) are used as the inputs to solve the inverse problem. In a real application, the measurement error is inevitable and a study on the robustness of the method is thus necessary. Suppose that we have the following (arbitrary) "measured" eigenfrequencies with errors:

$$R_1^* = 3.09604, \quad R_2^* = 6.22664, \quad R_3^* = 9.34938. \tag{22}$$

Compared with Eq. (17), the variations of the eigenfrequencies are tiny. Here we need to emphasize two things: (1) Since the mass (α) and tension variation (β) are very small, the corresponding *dimensionless* eigenfrequency variations are tiny. (2) Again, the eigenfrequencies in Eqs. (17) and (22) are dimensionless. As also discussed later, the micro/nanomechanical resonators are with very high resonant frequencies and those tiny shifts of the above dimensionless eigenfrequencies correspond to very large physical shifts. In one word, Eq. (22) actually represents relatively large measurement errors, which stands out by examining their relative eigenfrequency shifts. Similarly, Δ_j^*s, which are defined as $\Delta_j^* = (R_1^* - R_j^o)/R_j^o$, are given as follows:

$$\Delta_1^* = -1.45\%, \quad \Delta_2^* = -0.9\%, \quad \Delta_3^* = -0.8\%. \tag{23}$$

Compared with the actual exact shifts of Eq. (18), there are significant measurement errors as reflected by Eq. (23). The experimental error is indicated by the quantity defined as $(\Delta_j^* - \Delta_j)/\Delta_j$ and therefore, the measurement errors for the first, second and third eigenfrequencies are −4.32%, −7.14% and 4.76%, respectively. Now, those errored eigenfrequencies of Eq. (22) are used as the inputs and Eq. (21) yields the following:

$$\begin{cases} \mathcal{G}(R_1, \alpha, \xi_o, \beta, C) = \mathcal{G}(3.09604, \alpha, \xi_o, \beta, 10^{-3}) = 0, \\ \mathcal{G}(R_2, \alpha, \xi_o, \beta, C) = \mathcal{G}(6.22664, \alpha, \xi_o, \beta, 10^{-3}) = 0, \\ \mathcal{G}(R_3, \alpha, \xi_o, \beta, C) = \mathcal{G}(9.34938, \alpha, \xi_o, \beta, 10^{-3}) = 0. \end{cases} \tag{24}$$

Eq. (24) gives the result of (α, ξ_o, β)=$(1.107\times10^{-2}, 0.39381, -9.59257\times10^{-3})$. Compared with the exact result of (α, ξ_o, β)=$(10^{-2}, 0.4, -10^{-2})$, the errors are 10.7%, 4.0749% and −1.5485%, respectively. Clearly, the mass of α is significantly overestimated and the tension variation of β is slightly underestimated. The reason is that the measured first two eigenfrequencies are 4.32% and 7.14% smaller, respectively; a larger mass and a smaller tension reduction is a natural compensating mechanism for smaller "measured" eigenfrequencies. In the experimental measurement of eigenfrequencies, there are three scenarios: (1) all measured eigenfrequencies are larger (than the exact ones); (2) all measured eigenfrequencies are smaller; (3) some measured eigenfrequencies are larger and the others are smaller. For the first two scenarios, the errors of the results (i.e., α, ξ_o and β) as obtained by Eq. (15) are roughly proportional to the input errors. For the third scenario, the result errors can fluctuate significantly with the input ones. Several computational examples, which include all three scenarios, were conducted and none of the result errors were found to blow up. It seems that Eq. (15) provides a robust method of solving the inverse problem as the measurement errors vary.

The following two features of Schmid's inverse problem solving method [4] are noticed: (1) in their model, there are no effects of both damping and tension variation (i.e. $C=\beta=0$, which physically means that only the mass effect is accounted); (2) their method cannot work when $\alpha < 8.4\times10^{-3}$ or $\xi_o < 0.2$. In comparison, both Eqs. (10) and (15) include the damping and tension variation effects, which, besides the force sensing, provides a more accurate mass sensing. The second case is presented here to show that our inverse problem solving method has no problem of dealing with the scenarios of small adsorbate mass and its location close to the ends. In the second case, $\alpha=10^{-3}$, $\xi_o=0.1$, $\beta=-10^{-3}$ and $C=10^{-3}$ are set. The corresponding first three eigenfrequencies are now uniquely computed by Eq. (10) as the following

$$R_1 = 3.13997, \quad R_2 = 6.27787, \quad R_3 = 9.41391. \tag{25}$$

Compared with the first case, as α is smaller and ξ_o is closer to the end, the effect of adsorbate mass reduces significantly. Together with a smaller β, there are only tiny decrease of these three eigenfrequencies compared with R_j^o ($R_j^o = j\pi$ is the jth eigenfrequency of a string with no damping and adsorbate). With these three newly supplied eigenfrequencies, we repeat the above solution procedure and the following three equations are obtained

$$\begin{cases} \mathcal{G}(R_1, \alpha, \xi_o, \beta, C) = \mathcal{G}(3.13997, \alpha, \xi_o, \beta, 10^{-3}) = 0, \\ \mathcal{G}(R_2, \alpha, \xi_o, \beta, C) = \mathcal{G}(6.27787, \alpha, \xi_o, \beta, 10^{-3}) = 0, \\ \mathcal{G}(R_3, \alpha, \xi_o, \beta, C) = \mathcal{G}(9.41391, \alpha, \xi_o, \beta, 10^{-3}) = 0. \end{cases} \tag{26}$$

The three unknowns solved from the above equations are now (α, ξ_o, β)=(9.8924×10^{-4}, 0.10007155, -9.995×10^{-4}). Compared with the exact values of (α, ξ_o, β)=(10^{-3}, 0.1, -10^{-3}), the corresponding errors of α, ξ_o and β are −1.0768%, 0.7155% and 0.0492%, respectively. The relative errors of α and β are even smaller than those of the first case.

Because the whole inverse problem solving method is based on the fact that only one adsorbate on the string resonator, we need to address how the method can be used in a real application. The fundamental resonant frequency of a nanomechanical resonator is tens, hundreds of mega-hertz (MHz) or even giga-hertz (GHz) [7,8,11,26], therefore, the tiny fractional change of resonant frequency due to a tiny adsorbate is still absolutely large enough to be detected [15]. Furthermore, the current read-out technology has been continuously pushing the frequency resolution towards the range of parts-per-billion (ppb) for a nanomechanical resonator [56]. Nowadays, the state-of-art nanomechanical resonator is so sensitive to detect the shifts of resonant frequencies caused by the adsorption event of a molecule [7] or an atom [8,11]. The step-wise decreases of resonant frequencies measured in the experiments indicate the discrete nature of the molecules or atoms landing on the resonator surface one by one or cluster by cluster [7,8,11]. In the mass sensing tests of a nanomechanical resonator, there are tens, hundreds or even thousands adsorption events [7–11]. However, the total mass of the previously adsorbed analytes is very small compared with that of the resonator [26]; the incoming analyte is the dominant factor for the step-wise decrease of resonant frequencies as observed in the above experiments, which is the exact scenario for our method to apply.

4. Conclusion

The inverse problem of using the eigenfrequencies to determine the adsorbate mass, position and induced force is formulated and solved. By eliminating the off-diagonal elements in the mass matrix, an approximate analytical formula on the string resonant frequencies is derived, which is of great help to attacking the inverse problem. There are infinite combinations of the adsorbate mass, position and induced force which can result in the same shift of one resonant frequency. However, the three unknown parameters are uniquely determined by three resonant frequencies. Mathematically, three nonlinear equations are required to solve the inverse problem. Physically, the inverse problem can be solved because the three parameters impact on one resonant frequency differently and the shifts of different resonant frequencies are different to one another. Compared with the previous studies, the adsorbate-induced force and damping are included in the model, which causes some complexity on solving the inverse problem but provides a more accurate characterization on the effects induced by an adsorbate.

Acknowledgements

The research has been supported by the National Natural Science Foundation of China (NSFC No. 11372321). The authors are very thankful to the anonymous reviewer who brought up the robustness issue, which re-shaped our presentation and made the related discussion an important and inalienable part of this paper.

References

[1] K.L. Ekinci, Y.T. Yang, M.K. Roukes, J. Appl. Phys. 95 (2004) 2682.
[2] B. Ilic, H.G. Craighead, S. Krylov, W. Senaratne, C. Ober, P. Neuzil, J. Appl. Phys. 95 (2004) 3694.
[3] T. Larsen, S. Schmid, L.G. Villanueva, A. Boisen, ACS Nano 7 (2012) 6188.
[4] S. Schmid, S. Dohn, A. Boisen, Sensors 10 (2010) 8092.
[5] P.E. Sheehan, L.J. Whitman, Nano Lett. 5 (2005) 803.
[6] F. Schedin, A.K. Geim, S.V. Morozov, E.W. Hill, P. Blake, M.I. Katsnelson, K.S. Novoselov, Nat. Mater. 6 (2007) 652.
[7] J. Chaste, A. Eichler, J. Moser, G. Ceballos, R. Rurali, A. Bachtold, Nat. Nanotechnol. 7 (2012) 301.
[8] H. Chiu, P. Hung, H. Postma, M. Bockrath, Nano Lett. 8 (2008) 4342.
[9] A.K. Naik, M.S. Hanay, W.K. Hiebert, X.L. Feng, M.L. Roukes, Nat. Nanotechnol. 4 (2009) 445.
[10] M.S. Hanay, S. Kelber, A.K. Naik, D. Chi, S. Hentz, E.C. Bullard, E. Colinet, L. Duraffourg, M.L. Roukes, Nat. Nanotechnol. 7 (2012) 602.
[11] K. Jensen, K. Kim, A. Zettl, Nat. Nanotechnol. 3 (2008) 533.
[12] D.S. Kirkpatrickm, C. Denison, S.P. Gygi, Nat. Cell Biol. 7 (2005) 750.
[13] R. Aebersold, M. Mann, Nature 422 (2003) 198.
[14] B. Domon, R. Aebersold, Science 312 (2006) 212.
[15] R.G. Knobel, Nat. Nanotechnol. 3 (2008) 525.
[16] A. Boisen, Nat. Nanotechnol. 4 (2009) 404.
[17] T.P. Burg, M. Godin, S.M. Knudsen, W. Shen, G. Carlson, J.S. Foster, K. Babcock, S.R. Manalis, Nature 446 (2007) 1066.
[18] N.V. Lavrik, M.J. Sepaniak, P.G. Datskos, Rev. Sci. Instrum. 75 (2004) 2229.
[19] Y. Zhang, Sens. Actuators A 194 (2013) 169.
[20] L. Meirovitch, Analytical Methods in Vibrations, Macmillan Publishing Co. Inc., New York, 1967.
[21] G.Y. Chen, T. Thundat, E.A. Wachter, R.J. Warmack, J. Appl. Phys. 77 (1995) 3618.
[22] D. Ramos, J. Tamayo, J. Mertens, M. Calleja, A. Zaballos, J. Appl. Phys. 100 (2006) 106105.
[23] D. Ramos, J. Tamayo, J. Mertens, M. Calleja, L.G. Villanueva, A. Zaballos, Nanotechnology 19 (2006) 035503.
[24] Y. Zhang, Sens. Actuators B 202 (2014) 286.
[25] X. Huang, M. Manolidis, S. Jun, J. Hone, Appl. Phys. Lett. 86 (2005) 143104.
[26] Y. Zhang, Y.P. Zhao, Proc. R. Soc. A 469 (2013) 20140418.
[27] T. Ono, M. Esashi, Rev. Sci. Instrum. 76 (2005) 0930107.
[28] T. Thundat, E.A. Wachter, S.L. Sharp, R.J. Warmack, Appl. Phys. Lett. 66 (1995) 1695.
[29] E. Finot, A. Fabre, A. Passian, T. Thundat, Phys. Rev. Appl. 1 (2014) 024001.
[30] F.M. Battiston, J.P. Ramseyer, H.P. Lang, M.K. Baller, Ch. Gerber, J.K. Gimzewski, E. Meyer, H.J. Güntherodt, Sens. Actuators B 77 (2001) 122.
[31] H.C. McCaig, E. Myers, N.S. Lewis, M.L. Roukes, Nano Lett. 14 (2014) 3728.
[32] C. Li, T. Chou, Appl. Phys. Lett. 84 (2004) 5246.
[33] R. Chowdhury, S. Adhikari, J. Mitchell, Physica E 42 (2009) 104.
[34] J.W. Yan, K.M. Liew, L.H. He, Nanotechnology 24 (2013) 125703.
[35] J. Kehrbusch, E. Ilin, M. Hullin, E. Oesterschulze, Appl. Phys. Lett. 93 (2008) 023102.
[36] S. Dohn, W. Svendsen, A. Boisen, O. Hansen, Rev. Sci. Instrum. 78 (2007) 103303.
[37] Y. Zhang, Y. Liu, Sensors 14 (2014) 16296.
[38] A. Boisen, S. Dohn, S.S. Keller, S. Schmid, M. Tenje, Rep. Prog. Phys. 74 (2011) 036101.
[39] X. Wei, Q. Chen, S. Xu, L. Peng, J. Zuo, Adv. Funct. Mater. 19 (2009) 1753.
[40] Q.P. Unterreithmeier, T. Faust, J.P. Kotthaus, Phys. Rev. Lett. 105 (2010) 027205.
[41] S. Verbridge, D. Shapiro, H.G. Craighead, J.M. Parpia, Nano Lett. 7 (2007) 1728.
[42] S. Jun, X. Huang, M. Manolidis, A. Zorman, M. Mehregany, J. Hone, Nanotechnology 17 (2006) 1506.
[43] J. Moser, A. Eichler, J. Güttinger, M. Dykman, A. Bachtold, Nat. Nanotechnol. 9 (2014) 1007.
[44] S. Kim, H. Park, Nanotechnology 21 (2010) 1050710.
[45] V. Sazonova, Y. Yaish, H. Üstünel, D. Roundy, T. Arias, P.L. McEuen, Nature 431 (2004) 284.
[46] W. Conlay, A. Raman, C. Krousgrill, S. Mohammad, Nano Lett. 8 (2008) 1590.
[47] H. Üstünel, D. Roundy, T. Arias, Nano Lett. 5 (2005) 523.
[48] J. Mei, L. Li, Sens. Actuators B 188 (2013) 661.
[49] T. Murmu, S. Adhikari, Sens. Actuators B 188 (2013) 1319.
[50] Y. Zhang, J. Vib. Acoust. 133 (2011) 021006.
[51] Y. Zhang, K.D. Murphy, J. Sound Vib. 330 (2011) 5569.
[52] L. Meirovitch, Computational Methods in Structural Dynamics, Sijthoff & Noordhoff Inc., Maryland, 1980.
[53] K.D. Murphy, Y. Zhang, J. Sound Vib. 237 (2000) 319.
[54] Y. Zhang, L.J. Zhuo, H.S. Zhao, Proc. R. Soc. A 469 (2013) 20130449.
[55] W.H. Press, S.A. Teukolsky, W.T. Vetterling, B.P. Flannery, Numerical Recipes in Fortran, 2nd ed., Cambridge University Press, Cambridge, 1992.
[56] M. Modena, Y. Wang, D. Riedel, T.P. Burg, Lab Chip 14 (2014) 342.

Biographies

Yin Zhang, BS, Department of Mechanics, Peking University, Beijing, China, 1997 and PhD, Department of Mechanical Engineering, University of Connecticut, Storrs, Connecticut, USA, 2003. From 2003 to 2004, he worked as an assistant professor in the State Key Laboratory of Nonlinear Mechanics (LNM), Institute of Mechanics, Chinese Academy of Sciences (CAS) and as an associate professor from 2004-2012, and since 2012, as a professor. His current research focuses on the MEMS/NEMS structural mechanics, dynamics and the inverse problems in the sensors applications.

Ya-Pu Zhao received the PhD degree from the Department of Mechanics, Peking University, Beijing, China, in 1994. From 1994 to 1996, he was a postdoctoral associate with the Institute of Mechanics, Chinese Academy of Sciences (CAS). Since 1996, he has been working in the State Key Laboratory of Nonlinear Mechanics (LNM), Institute of Mechanics, CAS, and was promoted to full professor in 1998. His current technical interests include surface science, wetting, solid mechanics and nanomechanics.